

RC–HEOM Hybrid Method for Non-Perturbative Open System Dynamics

Po-Rong Lai,^{1,2} Jhen-Dong Lin,^{1,2} Yi-Te Huang,^{1,2} Po-Chen Kuo,³ Neill Lambert,⁴ and Yueh-Nan Chen^{1,2,5,*}

¹Department of Physics, National Cheng Kung University, Tainan 701, Taiwan

²Center for Quantum Frontiers of Research and Technology, NCKU, Tainan 701, Taiwan

³Department of Physics, National Pingtung University, Pingtung 900, Taiwan

⁴RIKEN Center for Quantum Computing (RQC), Wakoshi, Saitama 351-0198, Japan

⁵Physics Division, National Center for Theoretical Sciences, Taipei 106319, Taiwan

The Hierarchical equations of motion (HEOM) method is an important non-perturbative technique, allowing numerically exact treatment of open quantum systems with strong coupling and non-Markovian memory. However, its encoding of bath memory into auxiliary density operators often limits direct access to detailed bath information. In contrast, the reaction-coordinate (RC) mapping allows direct and transparent access to the dominant collective bath mode, but its perturbative and often Markovian treatment of the residual bath restricts its reliability. In this work, we introduce RC–HEOM, a hybrid method that unifies the strengths of both approaches by combining RC mapping with a fully non-perturbative HEOM description of the residual bath. RC–HEOM simultaneously retains exact non-Markovian memory and access to the RC mode, which enables analysis of system–RC information. Applying this method to the Anderson impurity models, we directly track the emergence of the Kondo singlet from the growth of the Kondo resonance and uncover a nontrivial RC-mediated coherence revival. These results demonstrate that RC–HEOM is a promising method for characterizing open quantum systems in regimes that are difficult to access with conventional master-equation methods.

Introduction— Open quantum systems research focuses on phenomena that occur when a system of interest interacts with a bath [1–4]. For memoryless baths or weak system-bath coupling, Lindblad master equation approaches provide good explanations for quantum phenomena [5–8]. However, if the system-bath coupling is too strong or memory effects are too profound, then the bath’s influence must be characterized by other approaches [9–11]. Existing methods that allow partial access to the system-bath joint state and enable calculations of system-bath correlations include time-evolving density operator with orthogonal polynomials [12, 13] and numerical renormalization group [14, 15]. These are chain-mapping approaches that map the bath into a chain of modes for calculations.

In recent years, development of reaction coordinate (RC) mapping in open quantum systems has shed light on an alternative approach towards obtaining bath information [16–23]. By using a Bogoliubov transformation on the bath operators, the system-bath Hamiltonian is mapped exactly into another Hamiltonian. *The Hamiltonian after RC mapping describes the system being coupled to the RC, which then couples to a residual bath.* Therefore, instead of solving the system dynamics when interacting with the bath, we can solve the system+RC dynamics when interacting with the residual bath. This allows us to obtain the system+RC joint state which provides information on the RC, the part of the bath that interacts with the system directly [16–23].

Currently, most of the works use Lindblad master equations to obtain the dynamics of the system+RC joint state, but this method has limitations such as the need for

a narrow bath spectral density [16, 17]. These limitations majorly come from the requirement of Born-Markov approximation when implementing Lindblad master equation [7]. The RC mapping can be implemented multiple times for a more favorable residual bath spectral density, at a cost of computation power [24]. As such, this approach is restricted to specific parameter regimes [17]. *To overcome these limitations, we consider a numerically exact treatment of the system+RC dynamics.*

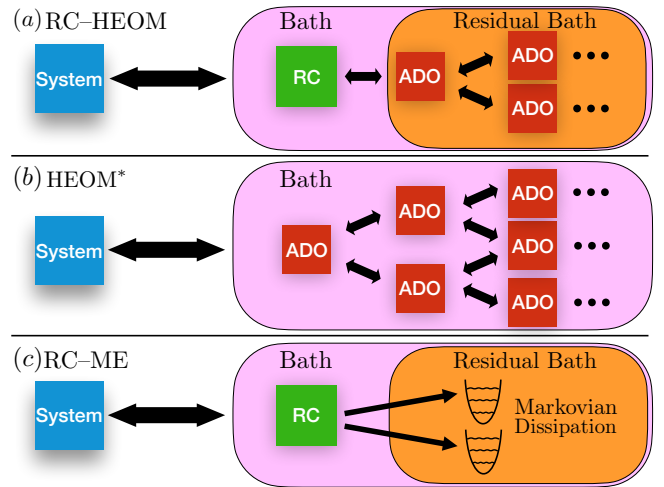


FIG. 1. Illustration of three methods used in open system dynamics calculations. (a) RC–HEOM. The system is coupled to the RC which couples to the ADOs of the residual bath. (b) HEOM*. System interactions with the bath is expressed as the system coupled to many ADOs. (c) RC–ME. The system is coupled to the RC which couples to the residual bath. System+RC interactions with the residual bath are treated with the Lindblad master equation.

* yuehnan@mail.ncku.edu.tw

In this letter, we develop a hybrid method that solves the system+RC dynamics exactly with the hierarchical equations of motion (HEOM [25–32], where the high-order system-bath correlations are captured by introducing auxiliary density operators (ADOs). Because *the HEOM method is numerically exact* for systems coupled to Gaussian baths, this enables us to obtain the exact system+RC joint state.

To demonstrate the advantages of using this hybrid method (labeled as RC–HEOM), we consider two examples. For both examples, we compare RC–HEOM results with the traditional way of treating the residual bath using Lindblad master equation (labeled RC–ME), as well as using HEOM to solve the system dynamics without implementing RC mapping (labeled as HEOM*). We use HEOM* results as benchmarks to ensure RC–HEOM results are correct in contrast to the results using RC–ME. We use RC–HEOM to access RC state information to calculate system-RC correlations. We illustrate the three methods used in Fig. 1. We note the difference between the three methods in Table. I.

In the first example, we explore Kondo resonance of the single-impurity Anderson model in the Kondo regime [33–37]. We find that RC–HEOM not only returns the correct density of states, but also allows us to calculate the singlet fraction [38]. We find that the singlet fraction increases as we lower the temperature, which indicates that the system+RC joint state is approaching the singlet state. In contrast, RC–ME fails to return the correct density of state to begin with. In the second example, we use RC–HEOM to explore the cause of bath mediated coherence revival in a two-impurity Anderson model [39–41]. Unlike HEOM*, which only visualizes the coherence revival, *RC–HEOM allows us to access system-bath coherence*. This enables us to understand how interference between effective system-bath coherence results in coherence revival of the two impurities.

TABLE I. Comparison of three methods.

	RC–HEOM	HEOM*	RC–ME
Numerically exact	✓	✓	✗
Computation speed	Slow	Slow	Fast
Access to Bath Information	all system-RC information	certain observables	all system-RC information

RC–HEOM method— We start by detailing the RC–HEOM method. We begin with the RC mapping for a system linearly coupled to either a bosonic or fermionic bath. Then, we show how to utilize HEOM to characterize the system+RC interactions with the residual bath.

First, the total Hamiltonian before RC mapping (setting $\hbar = 1$):

$$H_{\text{tot}} = H_{\text{sys}} + \sum_k \left(g_k c_k^\dagger s + \text{h.c.} \right) + \sum_k \omega_k c_k^\dagger c_k. \quad (1)$$

Here, H_{sys} is the Hamiltonian of the system mode s , g_k

is the coupling strength between the system and the k th bath mode, and c_k is the k th bath mode with ω_k being its eigenenergy. The RC mapping can be described by a Bogoliubov transformation on the bath operators [16–22]. We choose a set of creation and annihilation operators $C_k^{(\dagger)}$ via $C_k = \sum_l \Lambda_{kl} c_l$, where Λ is a unitary matrix with $\Lambda \Lambda^\dagger = \mathbb{1}$. These operators obey commutation (anti-commutation) relations for a bosonic (fermionic) bath. Further, the transformation satisfies two additional conditions:

$$\begin{cases} \lambda_0^* C_1 = \sum_k g_k^* c_k \\ \sum_k \omega_k \Lambda_{lk} \Lambda_{mk}^* \equiv \delta_{lm} E_l \quad \forall m \neq 1, l \neq 1. \end{cases} \quad (2)$$

The first relation yields the system-RC coupling λ_0 . The second relation generates the eigenenergy of the l th bath mode E_l ($l \geq 2$). After this RC mapping, the total Hamiltonian can be written as

$$H_{\text{tot}} = H_{\text{sys+RC}} + \sum_{l \neq 1} \left(T_l^* C_1^\dagger C_l + \text{h.c.} \right) + \sum_{l \neq 1} E_l C_l^\dagger C_l, \quad (3)$$

where $H_{\text{sys+RC}} = H_{\text{sys}} + \left(\lambda_0 C_1^\dagger s + \text{h.c.} \right) + E_1 C_1^\dagger C_1$. Here, we define $E_l \equiv \sum_k \omega_k |g_k|^2 / |\lambda_0|^2$ to be the RC eigenenergy and $T_l \equiv \sum_m \omega_m g_m \Lambda_{lm} / \lambda_0$ is the RC coupling strength with the l th residual bath mode. The system is now coupled to the RC mode C_1 which then couples to the l modes of the residual bath C_l ($l \geq 2$).

To obtain the system+RC joint state $\rho_{\text{sys+RC}}$, the RC–ME method considers Born-Markov approximation to obtain the following Lindblad master equation [16–19]:

$$\partial_t \rho_{\text{sys+RC}}(t) = -i[H_{\text{sys+RC}}, \rho_{\text{sys+RC}}] + \hat{\mathcal{D}}[\rho_{\text{sys+RC}}]. \quad (4)$$

Here, $\hat{\mathcal{D}}[\cdot] \equiv \sum_k \gamma_k [L_k \cdot L_k^\dagger - \{L_k^\dagger L_k, \cdot\} / 2]$ denotes the dissipator with decay rates γ_k and jump operators $L_k = |m\rangle \langle m| \hat{X} |n\rangle \langle n|$, where \hat{X} is the RC coupling operators (C_1, C_1^\dagger) and $|m\rangle, |n\rangle$ are the eigenstates of the system+RC. Notably, this approach remains valid only when the interaction between the RC and the residual bath is sufficiently weak.

If we instead employ RC–HEOM, which treats the residual bath interactions without approximations, the reduced density matrix of the system+RC joint state at time t can be written as

$$\rho_{\text{sys+RC}}(t) = \hat{\mathcal{T}} e^{\mathcal{F}(t)} \rho_{\text{sys+RC}}(0), \quad (5)$$

where $\hat{\mathcal{T}}$ is the time-ordering operator. Here, $\mathcal{F}(t)$ is the influence superoperator, which depends on the two-time correlation function $\mathcal{C}^\nu(t_1, t_2)$ of the residual bath and the RC mode C_1 [31, 42, 43].

In order to numerically solve Eq.(5) with HEOM, one usually expresses the two-time correlation functions as a sum of exponents: $\mathcal{C}^\nu(t_1, t_2) = \sum_{h=1}^N \eta_{\nu,h} e^{-\gamma_{\nu,h}(t_1-t_2)}$. This expression allows us to recursively differentiate the exponents in time to define local master equations for

ADOs $\rho_{\text{sys+RC}}^{\mathbf{q}}(t)$. Here, \mathbf{q} denotes a vector $[q_n, \dots, q_1]$ where each q_i represents a multi-index ensemble $\{\nu, h\}$. These ADOs capture the system-bath correlations exactly. Therefore, solving their equations of motion results in the system+RC joint state, which is $\rho_{\text{sys+RC}}^{|\mathbf{q}|=0}$. For $|\mathbf{q}| > 0$, the ADOs encode increasing orders of system-bath correlations. The RC-HEOM equations of motion can then be obtained:

$$\begin{aligned} \partial_t \rho_{\text{sys+RC}}^{\mathbf{q}}(t) = & -i[H_{\text{sys+RC}}, \rho_{\text{sys+RC}}^{\mathbf{q}}(t)] \\ & - \sum_{w=1}^n \gamma_{q_w} \rho_{\text{sys+RC}}^{\mathbf{q}}(t) - i \sum_{q'} \hat{\mathcal{A}}_{q'} \rho_{\text{sys+RC}}^{\mathbf{q}^+}(t) \\ & - i \sum_{w=1}^n \hat{\mathcal{B}}_{q_w} \rho_{\text{sys+RC}}^{\mathbf{q}_w^-}(t), \end{aligned} \quad (6)$$

where we use the multi-index notations: $\mathbf{q}^+ = [q', q_n, \dots, q_1]$ and $\mathbf{q}_w^- = [q_n, \dots, q_{w+1}, q_{w-1}, \dots, q_1]$. For fermions, we require $q' \notin \mathbf{q}$ due to the Pauli exclusion principle. In addition, the superoperators $\hat{\mathcal{A}}, \hat{\mathcal{B}}$ are used to describe system+RC interactions with the residual bath. They characterize how the $|\mathbf{q}|$ th level ADO ($|\mathbf{q}|$ is the length of vector \mathbf{q}) is coupled to the $|\mathbf{q}^+|$ th ADOs and the $|\mathbf{q}_w^-|$ th level ADOs. The mathematical details of the RC-HEOM formalism above and a bosonic example (since the two examples below work with fermionic systems) is shown in Supplemental Material [44]. The numerical simulations in the following are performed using HierarchicalEOM.jl [31] and QuantumToolbox.jl [45].

Example 1: Single impurity Anderson model— We explore the single impurity Anderson model (SIAM) using the RC-HEOM method. Starting from the total Hamiltonian of the SIAM (setting $\hbar = 1$):

$$\begin{aligned} H_{\text{tot}} = & H_{\text{sys}} + \sum_{n=\uparrow, \downarrow} \sum_k \left(g_k c_{k,n}^\dagger s_n \right. \\ & \left. + g_k^* s_n^\dagger c_{k,n} + \omega_k c_{k,n}^\dagger c_{k,n} \right), \end{aligned} \quad (7)$$

where $H_{\text{sys}} = \epsilon(s_\uparrow^\dagger s_\uparrow + s_\downarrow^\dagger s_\downarrow) + U s_\uparrow^\dagger s_\uparrow s_\downarrow^\dagger s_\downarrow$. Here, ϵ and U are respectively the eigenenergy and repulsion energy of the impurity. Subscript $n = \uparrow, \downarrow$ denotes spin. We consider the Lorentzian bath spectral density:

$$J_0(\omega) = \frac{\Gamma W^2}{(\omega - \mu)^2 + W^2} \quad (8)$$

with strength Γ , chemical potential μ , width W and $\omega \in (-\infty, \infty)$. This allows us to derive the RC parameters and residual bath spectral density: $|\lambda_0|^2 = \Gamma W/2, E_1 = \mu, J_1(\omega) = 2W$. We note that a flat residual spectral density is numerically difficult to implement using HEOM. Therefore, for the remainder of this letter, we employ an additional Lorentzian cutoff with sufficient width which returns the correct physics [44].

The SIAM has long been used for the study of Kondo physics [14, 33, 36, 37]. Particularly, both the formation of a Kondo singlet at zero temperature [14, 15] and

the temperature dependence of the Kondo resonance are well studied [46, 47]. Here, we take advantage of our RC-HEOM method to observe the singlet fraction F [38],

$$F = \langle \phi | \rho_{\text{sys+RC}}^\infty | \phi \rangle, \quad (9)$$

which can be used to estimate how close our system+RC steady state $\rho_{\text{sys+RC}}^\infty$ is to the singlet state $|\phi\rangle = \frac{1}{\sqrt{2}}(|\uparrow, \downarrow\rangle_{\text{sys,RC}} - |\downarrow, \uparrow\rangle_{\text{sys,RC}})$. This measure indicates the local Kondo screening correlations captured by the system+RC joint state. As temperature decreases, Kondo screening increases [48, 49], thus, we expect the singlet fraction to increase as well. To ensure our calculations are correct, we first check the density of states [50]

$$A(\omega) = \frac{1}{\pi} \int dt e^{i\omega t} \langle \{s_n(t), s_n^\dagger(0)\} \rangle \quad (10)$$

to ensure that results obtained via RC-HEOM match the benchmark calculations from HEOM*. In Fig. 2, we can see how the density of states obtained by HEOM* and RC-HEOM match up. The Kondo resonance increases as temperature drops as expected. We can also see that RC-ME is unable to produce the correct Kondo resonance, and the Hubbard resonance is not observable. This is due to our bath spectral density not being in the narrow structured regime opposite to the wide-band limit, where RC-ME is expected to be accurate [17]. We

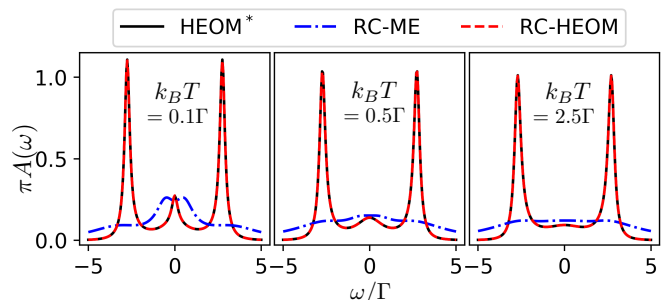


FIG. 2. The density of states $A(\omega)$ of the single impurity Anderson model at different temperatures. Lorentz bath parameters set to $W = 1.25\Gamma, \mu = 0$, and system parameters set to $U = 3\pi\Gamma/2, \epsilon = -U/2$. Results using HEOM*, RC-ME, RC-HEOM are shown in black solid, blue dashdot, red dashed curves, respectively. Computation details in Supplemental Material [44].

organize the results of the singlet fraction F in Table. II along with the Kondo resonance $A(\omega = 0)$. As temperature drops, the Kondo resonance grows, and the system+RC steady state approaches the spin singlet $|\phi\rangle$. These results demonstrate RC-HEOM's capability to explore Kondo physics.

Example 2: Bath mediated coherence revival in the two impurity Anderson model— The total Hamiltonian of the

TABLE II. Singlet fraction F and Kondo resonance $A(\omega = 0)$ for different temperatures.

$k_B T$	0.1Γ	0.5Γ	2.5Γ
$\pi A(\omega = 0)$	0.2741	0.1392	0.0935
$F(\text{RC-HEOM})$	0.2253	0.1754	0.0971

two-impurity Anderson model (TIAM) is written as:

$$H_{\text{tot}} = H_{\text{sys}} + \sum_{a=1,2} \sum_{n=\uparrow,\downarrow} \sum_k \left(g_k c_{k,n}^\dagger s_{n,a} + g_k^* s_{n,a}^\dagger c_{k,n} \right) + \sum_{n=\uparrow,\downarrow} \sum_k \omega_k c_{k,n}^\dagger c_{k,n}, \quad (11)$$

where $H_{\text{sys}} = \sum_{a=1,2} \epsilon_a (s_{\uparrow,a}^\dagger s_{\uparrow,a} + s_{\downarrow,a}^\dagger s_{\downarrow,a}) + U_a s_{\uparrow,a}^\dagger s_{\uparrow,a} s_{\downarrow,a}^\dagger s_{\downarrow,a}$. Here, ϵ_a and U_a are the eigenenergy and repulsion energy of impurity a , respectively. The bath spectral density is again Lorentzian. Notably, after RC mapping, the two impurities becomes coupled to a shared RC mode which then couples to the residual bath. Therefore, one can expect that the coherence between the two impurities could be mediated by the shared RC mode. To verify this intuition, we analyze the system coherence quantified by the l_1 norm [51]: $l_1^{\text{sys}} = \sum_{j \neq i}^{\dim\{H_{\text{sys}}\}} |\rho_{i,j}^{\text{sys}}|$ with respect to time t . Here, $\rho_{i,j}^{\text{sys}}$ is the matrix element of the system density operator in the local occupation basis of the two impurities. We plot l_1^{sys} in Fig. 3(a).

We find that the coherence dynamics using RC-HEOM agrees well with that of HEOM*, while the results using RC-ME does not. The key point of interest here is that HEOM* and RC-HEOM results both exhibit a sharp revival as indicated by a light gray vertical line at $Wt' = 97.9$.

To identify the origin of this revival, we decompose l_1^{sys} and analyze its individual compositions $|\rho_{i,j}^{\text{sys}}|$. We plot the compositions that display a revival in Fig. 3(b), as shown by the black, blue, red and green solid curves. We find that the black solid curve (along with its spin-down counterpart and conjugates that contribute identically) are the only coherence which exhibit a clear revival near t' . Because they connects states where each impurity hosts exactly one fermion before and after the jump, we refer to them as one-fermion (OF) coherence: $\langle \emptyset, \uparrow | \rho_{\text{sys}+\text{RC}} | \uparrow, \emptyset \rangle_{1,2}$, $\langle \uparrow, \emptyset | \rho_{\text{sys}+\text{RC}} | \emptyset, \uparrow \rangle_{1,2}$ and corresponding spin-down terms.

In order to check the significance of these OF coherence, we focus on

$$C_{\text{rev}} = \langle \emptyset, \uparrow | \rho_{\text{sys}+\text{RC}} | \uparrow, \emptyset \rangle_{1,2}, \quad (12)$$

as shown by the black solid curve in Fig. 3(b). We observe its change in value after t' : $|C_{\text{rev}}(t_\infty)| - |C_{\text{rev}}(t')| \approx 1.13 \times 10^{-3}$. Because the other OF coherence exhibit the same change over time as $|C_{\text{rev}}|$, this means their total change

is $\approx 4.52 \times 10^{-3}$. If we compare this value with the change in the l_1 norm after t' : $l_1^{\text{sys}}(t_\infty) - l_1^{\text{sys}}(t') \approx 2.97 \times 10^{-3}$, we can conclude that OF coherence are the dominant sources of coherence revival.

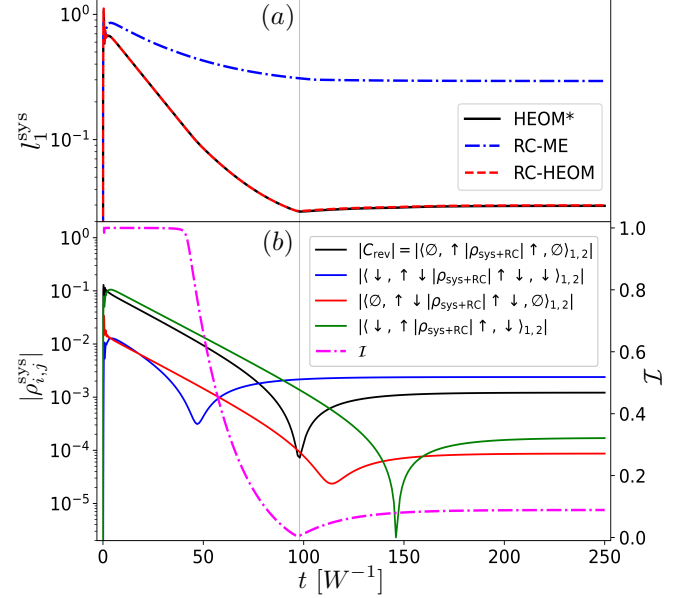


FIG. 3. Coherence revival of the two-impurity Anderson model. (a) l_1 norm of coherence for the two impurities: l_1^{sys} with respect to time t . Results using HEOM*, RC-ME, RC-HEOM are shown in black solid, blue dashdot, red dashed curves, respectively. Gray vertical line at t' indicates the coherence revival time. (b) Individual coherence contributions $|\rho_{i,j}^{\text{sys}}|$ (that make up l_1^{sys}) which display revival are shown in black, blue, red, and green solid curves. Additionally, the interference factor \mathcal{I} which measures the RC mediated path interference between the individual system+RC coherence that contribute to $|C_{\text{rev}}|$ (black solid curve) is shown as the magenta dashdot curve. Lorentz bath parameters are set to $\Gamma = 20W, \mu = 0, k_B T = 5W$, and system parameters are set to $\epsilon_1 = -2W, \epsilon_2 = -W, U_1 = U_2 = 10W$. Impurities are initialized in the vacuum state. RC is initialized in the thermal equilibrium state. Computation details are shown in Supplemental Material [44].

Next, we take advantage of RC-HEOM to access the RC's state information to understand how the RC mediates this revival. We decompose C_{rev} into its components: $C_{\text{rev}} = C_{\text{rev}}^{\text{vac}} + C_{\text{rev}}^{\uparrow} + C_{\text{rev}}^{\downarrow} + C_{\text{rev}}^{\uparrow\downarrow}$, where each term corresponds to the RC being in the vacuum, spin-up, spin-down and doubly occupied state, respectively (e.g. $C_{\text{rev}}^{\text{vac}} = \langle \emptyset, \uparrow, \emptyset | \rho_{\text{sys}+\text{RC}} | \uparrow, \emptyset, \emptyset \rangle_{1,2,RC}$). These four complex terms can interfere when we trace out the RC. Therefore, we can expect that $|C_{\text{rev}}|$ is also influenced by their interference.

To capture this effect, we consider the interference factor $\mathcal{I} \in [0, 1]$ defined as

$$\mathcal{I} \equiv \frac{|C_{\text{rev}}|}{|C_{\text{rev}}^{\text{vac}}| + |C_{\text{rev}}^{\uparrow}| + |C_{\text{rev}}^{\downarrow}| + |C_{\text{rev}}^{\uparrow\downarrow}|}, \quad (13)$$

where $\mathcal{I} = 1$ indicates perfect constructive interference,

whereas $\mathcal{I} = 0$ indicates perfect destructive interference. We plot \mathcal{I} against time in Fig. 3(b) as the magenta dash-dot curve. We can observe that $|C_{\text{rev}}|$ rises and falls in tandem with \mathcal{I} , which is determined by how the four system+RC coherence: $C_{\text{rev}}^{\text{vac}}, C_{\text{rev}}^{\uparrow}, C_{\text{rev}}^{\downarrow}, C_{\text{rev}}^{\uparrow\downarrow}$ interfere with each other.

We interpret the four system+RC coherence as the effective paths mediated by the RC to have a spin-up fermion jump from impurity 1 to impurity 2 (C_{rev}). Thus, the coherence revival originates from the overall interference of these paths changing from predominantly destructive to more constructive. The same mechanism applies to the other three OF coherence, so together they generate the revival of l_1 norm.

Conclusion—We have developed RC-HEOM, a hybrid method that combines reaction-coordinate mapping with a non-perturbative HEOM treatment of the residual bath. This approach preserves exact non-Markovian memory while providing explicit access to the reaction-coordinate mode, thereby going beyond the limitations of both methods. We apply RC-HEOM to both a single and double Anderson impurity model and demonstrate that the method can track the formation of the Kondo singlet and reveal RC-mediated coherence revival, offering detailed insight into the interplay between the sys-

tem and its environment. Overall, these results indicate that RC-HEOM is a useful and versatile tool for studying open quantum systems in regimes where conventional master-equation approaches are insufficient.

Given these features, the proposed RC-HEOM method could be particularly useful for enhancing ongoing studies on strongly coupled or non-Markovian quantum thermodynamic devices and heat engines [52–57], quantum transport [58–61], ultrastrong light-matter interactions [62–66], and non-Markovian heat and work statistics [67–69].

ACKNOWLEDGMENTS

This work is supported by the National Center for Theoretical Sciences and the National Science and Technology Council (NSTC), Taiwan, Grant No. NSTC 114-2112-M-006-015-MY3. P.-C. K. is supported by the National Science and Technology Council, Taiwan, under Grant No. NSTC 114-2112-M-153-004-MY3. N. L. is supported by MEXT KAKENHI Grant Numbers JP24H00816, JP24H00820.

-
- [1] H.-P. Breuer and F. Petruccione, *The theory of open quantum systems* (Oxford University Press on Demand, 2002).
- [2] G. Schaller, *Open Quantum Systems Far from Equilibrium*, Lecture Notes in Physics, Vol. 881 (Springer, Cham, 2014).
- [3] Á. Rivas and S. F. Huelga, *Open Quantum Systems: An Introduction* (Springer, Berlin, 2012).
- [4] U. Weiss, *Quantum Dissipative Systems*, 4th ed. (World Scientific, Singapore, 2012).
- [5] G. Lindblad, On the generators of quantum dynamical semigroups, *Commun. Math. Phys.* **48**, 119 (1976).
- [6] V. Gorini, A. Kossakowski, and E. C. G. Sudarshan, Completely positive dynamical semigroups of N -level systems, *J. Math. Phys.* **17**, 821 (1976).
- [7] D. Manzano, A short introduction to the Lindblad master equation, *AIP Adv.* **10**, 025106 (2020).
- [8] E. B. Davies, Markovian master equations, *Comm. Math. Phys.* **39**, 91 (1974).
- [9] H.-P. Breuer, E.-M. Laine, J. Piilo, and B. Vacchini, Colloquium: Non-Markovian dynamics in open quantum systems, *Rev. Mod. Phys.* **88**, 021002 (2016).
- [10] A. Rivas, S. F. Huelga, and M. B. Plenio, Quantum non-Markovianity: characterization, quantification and detection, *Rep. Prog. Phys.* **77**, 094001 (2014).
- [11] I. de Vega and D. Alonso, Dynamics of non-Markovian open quantum systems, *Rev. Mod. Phys.* **89**, 015001 (2017).
- [12] J. Prior, A. W. Chin, S. F. Huelga, and M. B. Plenio, Efficient simulation of strong system-environment interactions, *Phys. Rev. Lett.* **105**, 050404 (2010).
- [13] D. Tamascelli, A. Smirne, J. Lim, S. F. Huelga, and M. B. Plenio, Efficient Simulation of Finite-Temperature Open Quantum Systems, *Phys. Rev. Lett.* **123**, 090402 (2019).
- [14] R. Bulla, T. A. Costi, and T. Pruschke, Numerical renormalization group method for quantum impurity systems, *Rev. Mod. Phys.* **80**, 395 (2008).
- [15] K. G. Wilson, The renormalization group: Critical phenomena and the Kondo problem, *Rev. Mod. Phys.* **47**, 773 (1975).
- [16] N. Lambert, S. Ahmed, M. Cirio, and F. Nori, Modelling the ultra-strongly coupled spin-boson model with unphysical modes, *Nat. Commun.* **10**, 3721 (2019).
- [17] P. Strasberg, G. Schaller, T. L. Schmidt, and M. Esposito, Fermionic reaction coordinates and their application to an autonomous Maxwell demon in the strong-coupling regime, *Phys. Rev. B* **97**, 205405 (2018).
- [18] J. Iles-Smith, N. Lambert, and A. Nazir, Environmental dynamics, correlations, and the emergence of noncanonical equilibrium states in open quantum systems, *Phys. Rev. A* **90**, 032114 (2014).
- [19] N. Anto-Sztrikacs and D. Segal, Capturing non-Markovian dynamics with the reaction coordinate method, *Phys. Rev. A* **104**, 052617 (2021).
- [20] M. Shubrook, J. Iles-Smith, and A. Nazir, Non-Markovian quantum heat statistics with the reaction coordinate mapping, *Quant. Sci. Technol.* **10**, 025063 (2025).
- [21] C. L. Latune, Steady state in strong system-bath coupling regime: Reaction coordinate versus perturbative expansion, *Phys. Rev. E* **105**, 024126 (2022).
- [22] C. McConnell and A. Nazir, Strong coupling in thermoelectric nanojunctions: a reaction coordinate framework,

- New J. Phys.* **24**, 025002 (2022).
- [23] N. Anto-Sztrikacs, A. Nazir, and D. Segal, Effective-Hamiltonian Theory of Open Quantum Systems at Strong Coupling, *PRX Quantum* **4**, 020307 (2023).
- [24] R. Martinazzo, B. Vacchini, K. H. Hughes, and I. Burghardt, Communication: Universal Markovian reduction of Brownian particle dynamics, *J. Chem. Phys.* **134**, 011101M (2011).
- [25] Y. Tanimura and R. Kubo, Time Evolution of a Quantum system in Contact with a Nearly Gaussian-Markoffian Noise Bath, *J. Phys. Soc. Jpn.* **58**, 101 (1989).
- [26] Y. Tanimura, Nonperturbative expansion method for a quantum system coupled to a harmonic-oscillator bath, *Phys. Rev. A* **41**, 6676 (1990).
- [27] Y. Tanimura, Numerically “exact” approach to open quantum dynamics: The hierarchical equations of motion (HEOM), *J. Chem. Phys.* **153**, 020901 (2020).
- [28] J. Cao, L. Ye, R. Xu, X. Zheng, and Y. Yan, Recent advances in fermionic hierarchical equations of motion method for strongly correlated quantum impurity systems, *JUSTC* **53**, 0302 (2023).
- [29] Z. Li, N. Tong, X. Zheng, D. Hou, J. Wei, J. Hu, and Y. Yan, Hierarchical Liouville-Space Approach for Accurate and Universal Characterization of Quantum Impurity Systems, *Phys. Rev. Lett.* **109**, 266403 (2012).
- [30] N. Lambert, T. Raheja, S. Cross, P. Mencil, S. Ahmed, A. Pitchford, D. Burgarth, and F. Nori, QuTiP-BoFiN: A bosonic and fermionic numerical hierarchical-equations-of-motion library with applications in light-harvesting, quantum control, and single-molecule electronics, *Phys. Rev. Res.* **5**, 013181 (2023).
- [31] Y.-T. Huang, P.-C. Kuo, N. Lambert, M. Cirio, S. Cross, S.-L. Yang, F. Nori, and Y.-N. Chen, An efficient Julia framework for hierarchical equations of motion in open quantum systems, *Commun. phys.* **6**, 313 (2023).
- [32] M. Cirio, P. Liang, and N. Lambert, Input-output hierarchical equations of motion, *Phys. Rev. A* **112**, 012211 (2025).
- [33] P. W. Anderson, Localized magnetic states in metals, *Physical Review* **124**, 41 (1961).
- [34] T. A. Costi, A. C. Hewson, and V. Zlatić, Transport coefficients of the Anderson model via the numerical renormalization group, *J. Phys. Condens. Matter* **6**, 2519 (1994).
- [35] D. Goldhaber-Gordon, H. Shtrikman, D. Mahalu, D. Abusch-Magder, U. Meirav, and M. A. Kastner, Kondo effect in a single-electron transistor, *Nature* **391**, 156 (1998).
- [36] H. R. Krishna-murthy, J. W. Wilkins, and K. G. Wilson, Renormalization-group approach to the Anderson model of dilute magnetic alloys. ii. static properties for the asymmetric case, *Phys. Rev. B* **21**, 1044 (1980).
- [37] A. C. Hewson, *The Kondo Problem to Heavy Fermions*, Cambridge Studies in Magnetism (Cambridge University Press, Cambridge, 1993).
- [38] J. Modlawska and A. Grudka, Increasing singlet fraction with entanglement swapping, *Phys. Rev. A* **78**, 032321 (2008).
- [39] L. C. Andreani and H. Beck, Two-impurity Anderson model: A variational study, *Phys. Rev. B* **48**, 7322 (1993).
- [40] G. E. Santoro and G. F. Giuliani, Two-impurity Anderson model: Results of a perturbative expansion in U , *Phys. Rev. B* **49**, 6746 (1994).
- [41] F. Eickhoff, B. Lechtenberg, and F. B. Anders, Effective low-energy description of the two-impurity Anderson model: RKKY interaction and quantum criticality, *Phys. Rev. B* **98**, 115103 (2018).
- [42] M. Cirio, P.-C. Kuo, Y.-N. Chen, F. Nori, and N. Lambert, Canonical derivation of the fermionic influence superoperator, *Phys. Rev. B* **105**, 035121 (2022).
- [43] J.-D. Lin, P.-C. Kuo, N. Lambert, A. Miranowicz, F. Nori, and Y.-N. Chen, Non-Markovian quantum exceptional points, *Nat. Commun.* **16**, 1289 (2025).
- [44] See Supplemental Material at [URL will be inserted by publisher] for .
- [45] A. Mercurio, Y.-T. Huang, L.-X. Cai, Y.-N. Chen, V. Savona, and F. Nori, QuantumToolbox.jl: An efficient Julia framework for simulating open quantum systems, *Quantum* **9**, 1866 (2025).
- [46] K. Nagaoka, T. Jamneala, M. Grobis, and M. F. Crommie, Temperature Dependence of a Single Kondo Impurity, *Phys. Rev. Lett.* **88**, 077205 (2002).
- [47] A. Isidori, D. Roosen, L. Bartosch, W. Hofstetter, and P. Kopietz, Spectral function of the Anderson impurity model at finite temperatures, *Phys. Rev. B* **81**, 235120 (2010).
- [48] J. Shim, D. Kim, and H. S. Sim, Hierarchical entanglement shells of multichannel Kondo clouds, *Nat. Commun.* **14**, 3521 (2023).
- [49] N. H. Tu, D. Kim, M. L. Kim, J. Shim, R. Ito, D. Pomaranski, I. V. Borzenets, A. Ludwig, A. D. Wieck, H.-S. Sim, and M. Yamamoto, Electrical control of a Kondo spin screening cloud, [arXiv:2404.11955](https://arxiv.org/abs/2404.11955) (2025).
- [50] M. Cirio, N. Lambert, P. Liang, P.-C. Kuo, Y.-N. Chen, P. Mencil, K. Funo, and F. Nori, Pseudofermion method for the exact description of fermionic environments: From single-molecule electronics to the Kondo resonance, *Phys. Rev. Res.* **5**, 033011 (2023).
- [51] Y. Yuan, Z. Hou, J.-F. Tang, A. Streltsov, G.-Y. Xiang, C.-F. Li, and G.-C. Guo, Direct estimation of quantum coherence by collective measurements, *npj Quantum Inf.* **6**, 46 (2020).
- [52] C.-s. Yu and Q.-y. Zhu, Re-examining the self-contained quantum refrigerator in the strong-coupling regime, *Phys. Rev. E* **90**, 052142 (2014).
- [53] D. Gelbwaser-Klimovsky and A. Aspuru-Guzik, Strongly Coupled Quantum Heat Machines, *J. Phys. Chem. Lett.* **6**, 3477 (2015).
- [54] G. Katz and R. Kosloff, Quantum Thermodynamics in Strong Coupling: Heat Transport and Refrigeration, *Entropy* **18** (2016).
- [55] D. Newman, F. Mintert, and A. Nazir, Performance of a quantum heat engine at strong reservoir coupling, *Phys. Rev. E* **95**, 032139 (2017).
- [56] F. Ivander, N. Anto-Sztrikacs, and D. Segal, Strong system-bath coupling effects in quantum absorption refrigerators, *Phys. Rev. E* **105**, 034112 (2022).
- [57] M. Kaneyasu and Y. Hasegawa, Quantum Otto cycle under strong coupling, *Phys. Rev. E* **107**, 044127 (2023).
- [58] S. Restrepo, S. Böhlring, J. Cerrillo, and G. Schaller, Electron pumping in the strong coupling and non-markovian regime: A reaction coordinate mapping approach, *Phys. Rev. B* **100**, 035109 (2019).
- [59] C. W. Wächtler and G. Schaller, Transport through a quantum critical system: A thermodynamically consistent approach, *Phys. Rev. Res.* **2**, 023178 (2020).

- [60] N. Anto-Sztrikacs, F. Ivander, and D. Segal, Quantum thermal transport beyond second order with the reaction coordinate mapping, *J. Chem. Phys.* **156**, 214107 (2022).
- [61] G. T. Landi, D. Poletti, and G. Schaller, Nonequilibrium boundary-driven quantum systems: Models, methods, and properties, *Rev. Mod. Phys.* **94**, 045006 (2022).
- [62] M. Cirio, S. De Liberato, N. Lambert, and F. Nori, Ground State Electroluminescence, *Phys. Rev. Lett.* **116**, 113601 (2016).
- [63] M. Cirio, N. Shammah, N. Lambert, S. De Liberato, and F. Nori, Multielectron Ground State Electroluminescence, *Phys. Rev. Lett.* **122**, 190403 (2019).
- [64] S. De Liberato, Virtual photons in the ground state of a dissipative system, *Nat. Commun.* **8**, 1465 (2017).
- [65] R. Stassi, A. Ridolfo, O. Di Stefano, M. J. Hartmann, and S. Savasta, Spontaneous Conversion from Virtual to Real Photons in the Ultrastrong-Coupling Regime, *Phys. Rev. Lett.* **110**, 243601 (2013).
- [66] F. Beaudoin, J. M. Gambetta, and A. Blais, Dissipation and ultrastrong coupling in circuit QED, *Phys. Rev. A* **84**, 043832 (2011).
- [67] M. Popovic, M. T. Mitchison, A. Strathearn, B. W. Lovett, J. Goold, and P. R. Eastham, Quantum Heat Statistics with Time-Evolving Matrix Product Operators, *PRX Quantum* **2**, 020338 (2021).
- [68] L. Nicolin and D. Segal, Non-equilibrium spin-boson model: Counting statistics and the heat exchange fluctuation theorem, *J. Chem. Phys.* **135**, 164106 (2011).
- [69] M. Kilgour, B. K. Agarwalla, and D. Segal, Path-integral methodology and simulations of quantum thermal transport: Full counting statistics approach, *J. Chem. Phys.* **150**, 084111 (2019).

Supplemental Material for “RC–HEOM Hybrid Method for Non-perturbative Open System Dynamics”

Po-Rong Lai,^{1,2} Jhen-Dong Lin,^{1,2} Yi-Te Huang,^{1,2} Po-Chen Kuo,³ Neill Lambert,⁴ and Yueh-Nan Chen^{1,2,5}

¹*Department of Physics, National Cheng Kung University, Tainan 701, Taiwan*

²*Center for Quantum Frontiers of Research and Technology, NCKU, Tainan 701, Taiwan*

³*Department of Physics, National Pingtung University, Pingtung 900, Taiwan*

⁴*RIKEN Center for Quantum Computing (RQC), Wakoshi, Saitama 351-0198, Japan*

⁵*Physics Division, National Center for Theoretical Sciences, Taipei 106319, Taiwan*

DETAILS OF THE RC–HEOM FORMALISM

We show the mathematical details of the reaction coordinate (RC) mapping, derive the RC parameters and residual bath spectral density and disclose more information on the reaction coordinate–hierarchical equations of motion (RC–HEOM).

RC mapping

We start from the total Hamiltonian (setting $\hbar = 1$):

$$H_{\text{tot}} = H_{\text{sys}} + \sum_k \left(g_k c_k^\dagger s + \text{h.c.} \right) + \sum_k \omega_k c_k^\dagger c_k. \quad (1)$$

Here, H_{sys} is the Hamiltonian of the system with mode s , g_k is the coupling strength between the system mode and k th bath mode, and c_k is the k th bath mode with eigenenergy ω_k . We choose the bath spectral density to be $J_0(\omega) = 2\pi \sum_k |g_k|^2 \delta(\omega - \omega_k)$. We begin the RC mapping by performing a Bogoliubov transformation on the bath operators. We choose a set of creation and annihilation operators $C_k^{(\dagger)}$ via $C_k = \sum_l \Lambda_{kl} c_l$, where Λ is a unitary matrix with $\Lambda \Lambda^\dagger = \mathbf{1}$. These operators obey commutation (anti-commutation) relations when we’re working with a bosonic (fermionic) bath. Specifically, we choose the operators that satisfy two conditions:

$$\begin{cases} \lambda_0^* C_1 = \sum_k g_k^* c_k \\ \sum_k \omega_k \Lambda_{lk} \Lambda_{mk}^* \equiv \delta_{lm} E_l \quad \forall m \neq 1, l \neq 1. \end{cases} \quad (2)$$

The first condition generates

$$\sum_k \left(g_k c_k^\dagger s + \text{h.c.} \right) = \lambda_0 C_1^\dagger s + \text{h.c.}, \quad (3)$$

where λ_0 is the system-RC coupling strength. By making use of commutation or anti-commutation relations, we obtain

$$\begin{aligned} \lambda_0^* C_1 \lambda_0 C_1^\dagger \mp \lambda_0 C_1^\dagger \lambda_0^* C_1 &= |\lambda_0|^2 = \sum_k g_k^* c_k \sum_l g_l c_l^\dagger \mp \sum_l g_l c_l^\dagger \sum_k g_k^* c_k \\ &= \sum_{k,l} g_l g_k^* (c_k c_l^\dagger \mp c_l^\dagger c_k) = \sum_k |g_k|^2, \end{aligned} \quad (4)$$

where “ $-$ ” stands for commutation relation, “ $+$ ” stands for anti-commutation relation.

Thus, we connect the original system-bath coupling to the system-RC coupling.

By making use of the second condition in Eq.(2), we obtain

$$\sum_k \omega_k c_k^\dagger c_k = \sum_k \omega_k \sum_l \Lambda_{lk} C_l^\dagger \sum_m \Lambda_{mk}^\dagger C_m = \sum_{lm} C_l^\dagger C_m \sum_k \omega_k \Lambda_{lk} \Lambda_{mk}^\dagger. \quad (5)$$

We can deduce that

$$\begin{cases} C_1^\dagger C_1 \sum_k \omega_k \Lambda_{1k} \Lambda_{1k}^\dagger = C_1^\dagger C_1 \sum_k \frac{\omega_k |g_k|^2}{|\lambda_0|^2} = E_1 C_1^\dagger C_1 & \text{if } l = m = 1, \\ C_1^\dagger \sum_m C_m \sum_k \omega_k \Lambda_{1k} \Lambda_{mk}^\dagger = C_1^\dagger \sum_m C_m \sum_k \omega_k \frac{g_k^*}{\lambda_0^*} \Lambda_{mk}^\dagger = \sum_m T_m^* C_1^\dagger C_m & \text{if } l = 1, m \neq 1, \\ \sum_l C_l^\dagger C_1 \sum_k \omega_k \Lambda_{lk} \Lambda_{1k}^\dagger = \sum_l C_l^\dagger C_1 \sum_k \omega_k \frac{g_k}{\lambda_0} \Lambda_{lk} = \sum_l T_l C_l^\dagger C_1 & \text{if } l \neq 1, m = 1, \\ \sum_{lk} C_l^\dagger C_m \delta_{lm} E_l = \sum_l E_l C_l^\dagger C_l & \text{if } l \neq 1, m \neq 1, \end{cases} \quad (6)$$

which implies $\sum_k \omega_k c_k^\dagger c_k = E_1 C_1^\dagger C_1 + \sum_m T_m^* C_1^\dagger C_m + \sum_l T_l C_l^\dagger C_1 + \sum_l E_l C_l^\dagger C_l$, where we define $E_1 \equiv \sum_k \frac{\omega_k |g_k|^2}{|\lambda_0|^2}$ is the RC eigenenergy and $T_k \equiv \sum_m \frac{\omega_m g_m \Lambda_{km}}{\lambda_0}$ is the RC-residual bath coupling strength. Here, $E_l (l \geq 2)$ is the eigenenergy of the l th residual bath mode. Under these settings the total Hamiltonian after RC mapping is:

$$H_{\text{tot}} = H_{\text{sys+RC}} + \sum_{l \neq 1} \left(T_l^* C_1^\dagger C_l + \text{h.c.} \right) + \sum_{l \neq 1} E_l C_l^\dagger C_l, \quad (7)$$

where $H_{\text{sys+RC}} = H_{\text{sys}} + \left(\lambda_0 C_1^\dagger s + \text{h.c.} \right) + E_1 C_1^\dagger C_1$.

RC parameters and residual bath spectral density

Both the system-RC coupling strength and the RC eigenenergy as well as the residual bath spectral density can be expressed in terms of the bath spectral density $J_0(\omega) = 2\pi \sum_k |g_k|^2 \delta(\omega - \omega_k)$ (with cutoff frequencies ω_L and ω_R , such that $\omega \in [\omega_L, \omega_R]$). The system-RC coupling and RC eigenenergy are:

$$\begin{aligned} |\lambda_0|^2 &= \sum_k |g_k|^2 = \int_{\omega_L}^{\omega_R} \frac{d\omega}{2\pi} J_0(\omega), \\ E_1 &= \sum_k \frac{\omega_k |g_k|^2}{|\lambda_0|^2} = \int_{\omega_L}^{\omega_R} \frac{d\omega \omega J_0(\omega)}{2\pi |\lambda_0|^2}. \end{aligned} \quad (8)$$

To derive the residual bath spectral density $J_1(\omega) \equiv 2\pi \sum_{l \neq 1} |T_l|^2 \delta(\omega - E_l)$, we start with Heisenberg's equations of motion for Eq.(1):

$$\begin{aligned} \dot{s}(t) &= i[H_{\text{sys}}(t), s(t)] - i \sum_k g_k^* c_k(t) = -U_0(s) - i \sum_k g_k^* c_k(t), \\ \dot{c}_k(t) &= -ig_k s(t) - i\omega_k c_k(t), \end{aligned} \quad (9)$$

where an operator \mathcal{O} in the Heisenberg picture is $\mathcal{O}(t) = e^{-iH_{\text{tot}}t} \mathcal{O} e^{iH_{\text{tot}}t} (\hbar = 1)$ and $U_0(s) = -i[H_{\text{sys}}(t), s(t)]$. Next, by performing Fourier transform $\hat{f}(z) = \int_{-\infty}^{\infty} e^{izt} f(t) dt$, we get

$$\begin{cases} -iz\hat{s}(z) = -\hat{U}_0 - i \sum_k g_k^* \hat{c}_k(z) \\ -iz\hat{c}_k(z) = -ig_k \hat{s}(z) - i\omega_k \hat{c}_k(z). \end{cases} \quad (10)$$

Reorganizing terms around, we get

$$\hat{U}_0 = iz\hat{s}(z) + i \frac{W_0(z)}{2} \hat{s}(z), \quad (11)$$

where $W_0(z) \equiv 2 \sum_k \frac{|g_k|^2}{\omega_k - z} = \frac{1}{\pi} \int d\omega \frac{J_0(\omega)}{\omega - z}$. This gives us a W_0 function that links to J_0 . Now we link it to J_1 [1]. To do this, we write down Heisenberg's equations of motion for Eq.(7):

$$\begin{aligned} \dot{s}(t) &= -U_0(s) - i\lambda_0^* C_1(t), \\ \dot{C}_1(t) &= -i\lambda_0 s(t) - iE_1 C_1(t) - i \sum_{l \neq 1} T_l^* C_l(t), \\ \dot{C}_l(t) &= -iT_l C_1(t) - iE_l C_l(t). \end{aligned} \quad (12)$$

After Fourier transform, we have

$$\begin{aligned}
-iz\hat{s}(z) &= -\hat{U}_0 - i\lambda_0^*\hat{C}_1(z), \\
-iz\hat{C}_1(z) &= -i\lambda_0\hat{s}(z) - iE_1\hat{C}_1(z) - i\sum_{l\neq 1}T_l^*\hat{C}_l(z), \\
-iz\hat{C}_l(z) &= -iT_l\hat{C}_1(z) - iE_l\hat{C}_l(z).
\end{aligned} \tag{13}$$

Reorganizing terms around, we get

$$\hat{U}_0 = izs(z) + i\frac{|\lambda_0|^2\hat{s}(z)}{E_1 - z - W_1(z)/2}, \tag{14}$$

where $W_1(z) \equiv 2\sum_{l\neq 1}\frac{|T_l|^2}{E_l - z} = \frac{1}{\pi}\int d\omega\frac{J_1(\omega)}{\omega - z}$. The LHS of Eq.(11) and Eq.(14) are the same, which gives us the connection between W_0 and W_1

$$\frac{W_0(z)}{2} = \frac{|\lambda_0|^2}{E_1 - z - W_1(z)/2}. \tag{15}$$

The next step is to use Sokhotski-Plemelj theorem [2, 3]:

$$\lim_{\Delta\rightarrow 0^+}\int_{\omega_L}^{\omega_R}\frac{f(\omega')}{\omega' - \omega - i\Delta}d\omega' = i\pi f(\omega) + \mathcal{P}\int_{\omega_L}^{\omega_R}\frac{f(\omega')}{\omega' - \omega}d\omega'. \tag{16}$$

With \mathcal{P} being the Cauchy principal, this gives us

$$\begin{aligned}
\Im[W_0(\omega)] &= \Im\left[\lim_{\Delta\rightarrow 0^+}W_0(z = \omega + i\Delta)\right] = J_0(\omega), \\
\Im[W_1(\omega)] &= \Im\left[\lim_{\Delta\rightarrow 0^+}W_1(z = \omega + i\Delta)\right] = J_1(\omega).
\end{aligned} \tag{17}$$

Then, using Eq.(15), we obtain

$$J_1(\omega) = \frac{4|\lambda_0|^2 J_0(\omega)}{[\mathcal{P}\int_{\omega_L}^{\omega_R}\frac{1}{\pi}\frac{J_0(\omega')}{\omega' - \omega}d\omega']^2 + J_0(\omega)^2}. \tag{18}$$

Using Eq.(8) and Eq.(18), we can derive that $|\lambda_0|^2 = \Gamma W/2$, $E_1 = \mu$, $J_1(\omega) = 2W$ for a initial Lorentz spectral density $J_0(\omega) = \Gamma W^2/[(\omega - \mu)^2 + W^2]$ ($\omega \in (-\infty, \infty)$) in our main text.

HEOM and equations of motion for ADOs

For our RC-HEOM method, we treat the residual bath interaction with HEOM. Without approximations, the reduced density matrix of the system+RC joint state at time t can be written in terms of the Dyson series [4]:

$$\rho_{\text{sys+RC}}(t) = \hat{\mathcal{T}}e^{\mathcal{F}(t)}\rho_{\text{sys+RC}}(0) = \hat{\mathcal{T}}\exp\left\{-\int_0^t dt_1 \int_0^{t_1} dt_2 \hat{\mathcal{W}}(t_1, t_2)[\rho_{\text{sys+RC}}(0)]\right\}, \tag{19}$$

where $\hat{\mathcal{T}}$ is the time-ordering operator. Here, $\mathcal{F}(t)$ is the influence superoperator and a function of the two-time correlation function $\mathcal{CF}^\nu(t_1, t_2)$ and the RC mode C_1 . The explicit form for $\hat{\mathcal{W}}$ for bosonic and fermionic baths are:

$$\begin{aligned}
\hat{\mathcal{W}}(t_1, t_2)[\cdot] &= \sum_{p=\pm}\sum_{\nu=\pm}\left\{\mathcal{CF}^\nu(t_1, t_2)[C_1^{\bar{\nu}}(t_1), C_1^\nu(t_2) \cdot]_{-p} + \mathcal{CF}^\nu(t_2, t_1)[\cdot, C_1^{\bar{\nu}}(t_2), C_1^\nu(t_1)]_{-p}\right\} \text{ for fermions,} \\
\hat{\mathcal{W}}(t_1, t_2)[\cdot] &= \sum_{\nu=\pm}\left\{\mathcal{CF}^\nu(t_1, t_2)[C_1^{\bar{\nu}}, C_1^\nu(t_2) \cdot]_{-} - \mathcal{CF}^\nu(t_2, t_1)[C_1^{\bar{\nu}}(t_1), \cdot, C_1^\nu(t_2)]_{-}\right\} \text{ for bosons,}
\end{aligned} \tag{20}$$

where ν denotes the presence ($\nu = +$) or absence ($\nu = -$) of Hermitian conjugation and $\bar{\nu} := -\nu$. Here, $[\cdot, \cdot]_{-}$ and $[\cdot, \cdot]_{+}$ represent the commutator and anti-commutator to keep track of the parity p .

Here, \mathcal{CF}^ν is the two-time correlation function for absorption ($\nu = +$) and emission ($\nu = -$) processes. We can express the correlation functions with the residual bath spectral density $J_1(\omega)$ [5, 6]

$$\begin{aligned} \mathcal{CF}^{\nu=+}(t_1, t_2) &= \int_{\omega_L}^{\omega_R} \frac{d\omega}{2\pi} J_1(\omega) n_{\text{FD}}^{\text{Eq}}(\omega) e^{i\omega(t_1-t_2)}, \quad \mathcal{CF}^{\nu=-}(t_1, t_2) = \int_{\omega_L}^{\omega_R} \frac{d\omega}{2\pi} J_1(\omega) (1 - n_{\text{FD}}^{\text{Eq}}(\omega)) e^{-i\omega(t_1-t_2)} \text{ for fermions,} \\ \mathcal{CF}^{\nu=+}(t_1, t_2) &= \int_{\omega_L}^{\omega_R} \frac{d\omega}{2\pi} J_1(\omega) n_{\text{BE}}^{\text{Eq}}(\omega) e^{i\omega(t_1-t_2)}, \quad \mathcal{CF}^{\nu=-}(t_1, t_2) = \int_{\omega_L}^{\omega_R} \frac{d\omega}{2\pi} J_1(\omega) (1 + n_{\text{BE}}^{\text{Eq}}(\omega)) e^{-i\omega(t_1-t_2)} \text{ for bosons,} \end{aligned} \quad (21)$$

where $n_{\text{FD}}^{\text{Eq}}(\omega)$ ($n_{\text{BE}}^{\text{Eq}}(\omega)$) is the Fermi-Dirac (Bose-Einstein) distribution. We can now see how the two-time correlation functions \mathcal{CF}^ν capture the bath effects.

In order to numerically solve Eq.(19) with HEOM, we usually express the two-time correlation functions as a sum of exponents: $\mathcal{CF}^\nu(t_1, t_2) = \sum_{h=1}^N \eta_{\nu,h} e^{-\gamma_{\nu,h}(t_1-t_2)}$. This expression allows us to recursively differentiate the exponents in time to define local master equations for ADOs $\rho_{\text{sys+RC}}^{\mathbf{q}}(t)$. Here, \mathbf{q} denotes a vector $[q_n, \dots, q_1]$, where each q_i represents a multi-index ensemble $\{\nu, h\}$. These ADOs capture the system-bath correlations exactly, so solving their equation of motion results in the system+RC joint state, which is $\rho_{\text{sys+RC}}^{|\mathbf{q}|=0}$. For $|\mathbf{q}| > 0$, the ADOs encode increasing orders of system-bath correlations. The RC-HEOM equations of motion are:

$$\partial_t \rho_{\text{sys+RC}}^{\mathbf{q}}(t) = -i[H_{\text{sys+RC}}, \rho_{\text{sys+RC}}^{\mathbf{q}}(t)] - \sum_{w=1}^n \gamma_{q_w} \rho_{\text{sys+RC}}^{\mathbf{q}}(t) - i \sum_{q'} \hat{\mathcal{A}}_{q'} \rho_{\text{sys+RC}}^{\mathbf{q}^+}(t) - i \sum_{w=1}^n \hat{\mathcal{B}}_{q_w} \rho_{\text{sys+RC}}^{\mathbf{q}_w^-}(t), \quad (22)$$

where we use multi-index notations: $\mathbf{q}^+ = [q', q_n, \dots, q_1]$, $\mathbf{q}_w^- = [q_n, \dots, q_{w+1}, q_{w-1}, \dots, q_1]$. For fermions, we additionally require $q' \notin \mathbf{q}$. Equation.(22) uses superoperators $\hat{\mathcal{A}}, \hat{\mathcal{B}}$ to describe system+RC interactions with the residual bath. They display how the $|\mathbf{q}|$ th level ADO ($|\mathbf{q}|$ is the length of vector \mathbf{q}) is coupled to the $|\mathbf{q}^+|$ th ADOs and the $|\mathbf{q}_w^-|$ th level ADOs. Their explicit forms are as follows:

$$\begin{aligned} \hat{\mathcal{A}}_{q'}[\cdot] &= C_1^{\bar{\nu}}[\cdot] - [\cdot] C_1^{\bar{\nu}}, \quad \hat{\mathcal{B}}_{q_w}[\cdot] = (-1)^{n-w} (\eta_{\nu,h} C_1^\nu[\cdot] - (\eta_{\nu,h}^{\bar{\nu}})^* [\cdot] C_1^\nu) \text{ for fermions,} \\ \hat{\mathcal{A}}_{q'}[\cdot] &= C_1^{\bar{\nu}}[\cdot] - [\cdot] C_1^{\bar{\nu}}, \quad \hat{\mathcal{B}}_{q_w}[\cdot] = \eta_{\nu,h}^\nu C_1^\nu[\cdot] - (\eta_{\nu,h}^{\bar{\nu}})^* [\cdot] C_1^\nu \text{ for bosons.} \end{aligned} \quad (23)$$

RC-HEOM COMPUTATION DETAILS

Lorentz cutoff for residual bath spectral density

When working with the single impurity Anderson model (SIAM) or two impurity Anderson model (TIAM) model coupled to a Lorentzian bath with the RC-HEOM method, we calculate the residual bath spectral density to be $J_1(\omega) = 2W$, which is a constant. In this scenario, the two-time correlations functions would be

$$\mathcal{CF}^{\nu=+}(t) = W\delta(t) - \frac{iW e^{i\mu t}}{\beta \sinh \frac{t\pi}{\beta}} \text{ and } \mathcal{CF}^{\nu=-}(t) = W\delta(t) - \frac{iW e^{-i\mu t}}{\beta \sinh \frac{t\pi}{\beta}}. \quad (24)$$

Unfortunately, there is no way of expressing the Dirac delta function $\delta(t)$ as a finite sum of exponents for us to use in HEOM. To circumvent this, instead of using $J_1(\omega) = 2W$, we apply a Lorentzian cutoff so the residual bath spectral density looks like

$$J_1'(\omega) = \frac{2W \cdot \Delta}{\omega^2 + \Delta^2}, \text{ where } \Delta \gg W, \quad (25)$$

which is effectively a very wide Lorentz spectral density as a replacement. This way, we can utilize the built in functions from HierarchicalEOM.jl to express the correlation functions as a sum of exponents and perform HEOM calculations [5].

To ensure that this replacement does not damage the integrity of our calculations, we compared key metrics with HEOM* results in our main text. We checked the density of states $A(\omega) = \frac{1}{\pi} \int dt e^{i\omega t} \langle \{s_n(t), s_n^\dagger(0)\} \rangle$ in Example 1 and checked the coherence dynamics in Example 2.

HEOM computation parameters

In Table I, we detail the computation parameters when using HEOM to generate the results in Example 1. The amount of memory and computation time needed to perform the calculations is decided by the size of the HEOM Liouvillian superoperator (HEOMs) matrix. The HEOMs matrix size is determined by "system dimension² × number of ADOs" [5]. The number of auxiliary density operators (ADOs) is decided by the number of exponents used to fit the correlation function N_{exp} and the maximum level of ADO we incorporate ($|\mathbf{q}_{\text{max}}|$, known as the hierarchical tier or tier). The tables below show the N_{exp} required to get a good fit of the correlation functions, whilst "tier" shows the number of hierarchical tiers necessary to reach convergence up to some small error.

TABLE I. HEOM computation parameters for Example 1 in the main text.

	$k_B T$	system dimension	N_{exp}	tier	ADOs	HEOMs matrix size
HEOM*	0.2	4	4	3	1351	21,616
RC-HEOM	0.2	16	4	4	6196	1,586,176
HEOM*	1	4	4	3	1351	21,616
RC-HEOM	1	16	4	3	1351	345,856
HEOM*	5	4	2	2	79	1264
RC-HEOM	5	16	2	2	79	20,224

In Table II, we detail the computation parameters when using HEOM to generate the results in Example 2.

TABLE II. HEOM computation parameters for Example 2 in the main text

	system dimension	N_{exp}	tier	ADOs	HEOMs matrix size
HEOM*	16	2	5	1586	406,016
RC-HEOM	64	6	2	407	1,667,072

EXAMPLE OF USING RC-HEOM FOR BOSONIC SYSTEMS

We demonstrate how our RC-HEOM method can also work for bosonic systems. We demonstrate how we can obtain the correct system dynamics for the spin boson model with rotating wave approximation (RWA), i.e. the multi-mode Jaynes-Cummings model, when reaction coordinate-master equation (RC-ME) fails.

We start by performing the RC mapping on the model Hamiltonian:

$$H_{\text{tot}} = H_{\text{sys}} + \sum_k \left(g_k \sigma_- b_k^\dagger + g_k^* b_k \sigma_+ \right) + \sum_k \omega_k b_k^\dagger b_k \quad (26)$$

Here, $H_{\text{sys}} = \frac{\omega_q}{2} \sigma_z + \frac{\Delta}{2} \sigma_x$ is the system Hamiltonian with qubit splitting ω_q and tunneling matrix element Δ . Note that σ_\pm are the system raising and lowering operators, g_k is the system-bath coupling strength, b_k is the k th mode of the bath with eigenenergy ω_k . The system-bath correlations can be fully described by the spectral density $J_0(\omega) = 2\pi \sum_k |g_k|^2 \delta(\omega - \omega_k)$.

After RC mapping, the Hamiltonian is

$$H = H_{\text{sys}} + \lambda_0 s B_1^\dagger + \lambda_0^* B_1 s^\dagger + E_1 B_1^\dagger B_1 + \sum_{l \neq 1} \left(T_l^* B_1^\dagger B_l + T_l B_l^\dagger B_1 \right) + \sum_{l \neq 1} E_l B_l^\dagger B_l, \quad (27)$$

where E_1 is the RC eigenenergy, T_l is the coupling strength between the RC mode B_1 and the l th bath mode B_l ($l \geq 2$), the latter with eigenenergy E_l . From Eq.(27) we can see that the system is now coupled to the RC which then couples to the l modes of the residual bath with spectral density $J_1(\omega) = 2\pi \sum_{k \neq 1} |T_k|^2 \delta(\omega - E_k)$.

For our example, we choose the under-damped Brownian motion spectral density:

$$J_0(\omega) = \frac{\gamma \lambda^2 \omega}{(\omega^2 - \omega_0^2)^2 + \gamma^2 \omega^2}, \quad (28)$$

where $\omega \in [0, \infty)$ and $\omega_0, \gamma, \lambda$ are the resonant frequency, width and strength of the bath, respectively. From which, we can derive the parameters of the Hamiltonian after reaction coordinate mapping:

$$\begin{aligned} |\lambda_0|^2 &= \frac{\lambda^2}{\pi \sqrt{4\omega_0^2 - \gamma^2}} \tan^{-1} \frac{\sqrt{4\omega_0^2 - \gamma^2}}{\gamma}, \\ E_1 &= \frac{\lambda^2}{4|\lambda_0|^2}, \\ J_1(\omega) &= \frac{4|\lambda_0|^2 J_0}{\left(\frac{\omega_0^2 - \omega^2}{\gamma\omega} J_0 - \bar{p}(\omega)\right)^2 + J_0^2}, \end{aligned} \quad (29)$$

where $\bar{p}(\omega) = \mathcal{P} \int_{-\infty}^0 \frac{1}{\pi} \frac{J_0(\omega')}{\omega' - \omega} d\omega'$. Note that $\bar{p}(\omega)$ is solved numerically instead of the first term in the denominator in Eq.(18). This is due to ω being positive in our example, so solving $\bar{p}(\omega)$ numerically is much easier because we don't integrate over any poles.

Next, we implement HEOM to obtain the system+RC dynamics when interacting with the residual bath. We use the bosonic two-time correlation functions from Eq.(21). The absorption and emission correlation functions must each be approximated as a sum of exponents to obtain the ADOs for HEOM calculation. To do so, we use the AAA algorithm to express $J_1(\omega), n_{\text{BE}}^{\text{Eq}}(\omega)$ in barycentric form [7]. Their poles are then used to express \mathcal{CF}^ν as a sum of exponents [8].

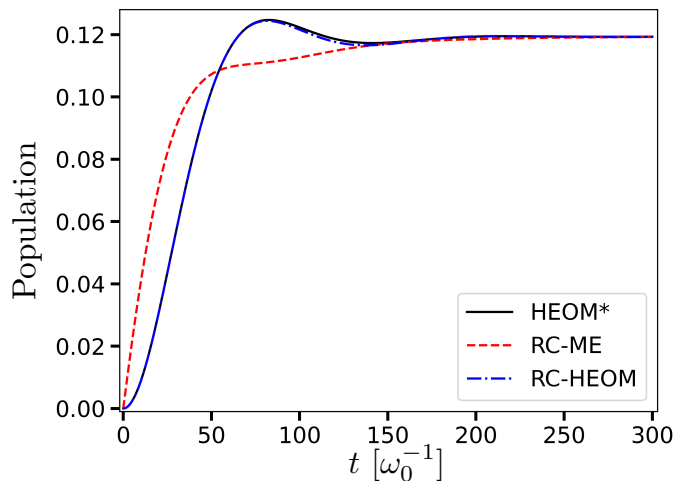


FIG. 1. System population with respect to time t . Black solid curve is the result using HEOM*, representing the correct dynamics. Red dashed curve is the result using RC-ME. Blue dashdot curve is the result using RC-HEOM. RC-HEOM recovers the correct short-time dynamics, whereas RC-ME does not, as seen in comparison with HEOM*.

We now look at the population dynamics when using RC-ME, HEOM* and RC-HEOM. We choose the bath spectral density parameters to be $\gamma = 0.05\omega_0, \lambda = 0.05\omega_0$ and set its temperature to be $k_B T = 0.5\omega_0$. The system parameters are $\omega_q = \omega_0, \Delta = 0$. We set the initial state of the system to be in its ground state, the RC in its thermal equilibrium state at temperature T . We plot the population dynamics against time t (in units of ω_0^{-1}) in Fig.1. We find that when the population stabilizes, the results are the same for each method at around 0.119. However, RC-ME (red dashed) is unable to produce the correct short-time population dynamics. In contrast, using RC-HEOM (blue dashdot), the result is nearly identical to HEOM* (black solid).

In Table III below, we detail the computation parameters used to generate the results in Fig.1. We write the system dimension when we use RC-HEOM as 2×4 to emphasize that the RC dimension here is 4. This means that it can have up to 3 bosons. This is the cutoff boson count that converges.

s

[1] P. Strasberg, G. Schaller, T. L. Schmidt, and M. Esposito, Fermionic reaction coordinates and their application to an autonomous Maxwell demon in the strong-coupling regime, *Phys. Rev. B* **97**, 205405 (2018).

TABLE III. HEOM computation parameters for bosonic example

	system dimension	N_{exp}	tier	ADOs	HEOMs	matrix size
HEOM*	2	88	3	121,485		485,940
RC-HEOM	2×4	256	2	33,153		2,121,792

- [2] H. E. Haber, The Sokhotski–Plemelj Formula, Lecture notes, University of California, Santa Cruz (2017).
- [3] H.-P. Breuer and F. Petruccione, *The theory of open quantum systems* (Oxford University Press on Demand, 2002).
- [4] M. Cirio, P.-C. Kuo, Y.-N. Chen, F. Nori, and N. Lambert, Canonical derivation of the fermionic influence superoperator, *Phys. Rev. B* **105**, 035121 (2022).
- [5] Y.-T. Huang, P.-C. Kuo, N. Lambert, M. Cirio, S. Cross, S.-L. Yang, F. Nori, and Y.-N. Chen, An efficient Julia framework for hierarchical equations of motion in open quantum systems, *Commun. phys.* **6**, 313 (2023).
- [6] J.-D. Lin, P.-C. Kuo, N. Lambert, A. Miranowicz, F. Nori, and Y.-N. Chen, Non-Markovian quantum exceptional points, *Nat. Commun.* **16**, 1289 (2025).
- [7] Y. Nakatsukasa, O. Sète, and L. N. Trefethen, The AAA Algorithm for Rational Approximation, *SIAM J. Sci. Comput.* **40**, A1494 (2018).
- [8] M. Xu, Y. Yan, Q. Shi, J. Ankerhold, and J. T. Stockburger, Taming quantum noise for efficient low temperature simulations of open quantum systems, *Phys. Rev. Lett.* **129**, 230601 (2022).